J Solid State Electrochem (2011) 15:2239–2251
DOI 10.1007/s10008-010-1243-1

ORIGINAL PAPER

# Formation, surface characterization, and electrocatalytic application of self-assembled monolayer films of tetra-substituted manganese, iron, and cobalt benzylthio phthalocyanine complexes

**Isaac Adebayo Akinbulu · Kenneth Iyke Ozoemena · Tebello Nyokong**

Received: 23 April 2010 / Revised: 8 November 2010 / Accepted: 9 November 2010 / Published online: 25 November 2010


**Abstract** Molecular thin films of manganese (SAM-**2**), iron (SAM-**3**), and cobalt (SAM-**4**) phthalocyanine complexes, non-peripherally tetra-substituted with benzylmercapto, were formed on polycrystalline gold disc electrode by self-assembly technique. Surface characteristics of the films were interrogated by cyclic voltammetry. Significant passivation of voltammetry processes associated with bare gold surface (gold oxidation and underpotential deposition of copper) confirmed formation of the films. Electrocatalytic property of the films was evidenced from better voltammetry responses (less positive oxidation potential and better current signal) of the insecticide, carbofuran, on these films, relative to that on bare gold electrode. In terms of less positive oxidation potential, the FePc derivative (**3**) gave the best response, while the best current signal was observed on SAM-**2**-modified gold electrode. The average heterogeneous rate constant, $k$, for the oxidation of carbofuran was $3.6\times10^{-2}$ cm $s^{-1}$ on the SAM film with the best current signal (SAM-**2**).

**Keywords** Manganese · Iron · Cobalt · Benzylthio phthalocyanine · Self-assembled monolayer · Carbofuran

I. A. Akinbulu · K. I. Ozoemena · T. Nyokong (✉)
Department of Chemistry, Rhodes University,
Grahamstown 6140, South Africa
e-mail: t.nyokong@ru.ac.za

I. A. Akinbulu
e-mail: isaacbayo.akinbulu@gmail.com

K. I. Ozoemena
Materials Science & Manufacturing,
Council for Scientific & Industrial Research (CSIR),
Pretoria 0001, South Africa
e-mail: ozoemena@csir.co.za

## Introduction

Self-assembled monolayer (SAM) films of organic materials have found widespread applications in molecular electronic devices [1, 2], corrosion prevention [3–5], design of electrochemical- and bio-sensors [6–10], electrocatalysis [11–14], photochemical [15], and electrochemical [16] processes. Self-assembled monolayers may be formed on a variety of electrodes, including: chlorosilane on silicon [17], carboxylic acids on metal oxides [18], and thiol-derivatised organic compounds on gold [19–22]. Self-assembled monolayer films of organosulfur compounds formed on gold are the most extensively studied. This can be attributed to the relative inertness of gold, specific and strong interaction of sulfur with gold, and ease of preparation and characterization of SAMs on gold [23].

SAMs formed from sulfur containing metallophthalocyanine (MPc) complexes have been intensively studied [11–14, 24–27]. Interest in SAMs of these macrocyclic complexes is focused on investigation of their possible orientation on a given substrate [24–27], which impacts significantly on their likely applications. Most importantly, their electrocatalytic properties towards various analytes have also elicited keen interest [11–14]. In the present work, we report on the formation and surface characterization of the SAMs of non-peripherally tetra-substituted manganese (**2**) iron (**3**), and cobalt (**4**) benzylmercapto phthalocyanine complexes (Scheme 1) on gold. The synthesis and electrochemical behavior of complex **4** was recently reported [28] while the synthesis and electrochemical characterization of complexes **2** and **3** are reported in this work. Surface characteristics of the SAM films were studied by cyclic voltammetry. SAMs formed from aryl- and alkyl-thio MPc complexes have been reported, without cleavage of the aryl or alkyl group [11].

**Scheme 1** Synthetic pathway for complexes **2**, **3**, and **4**

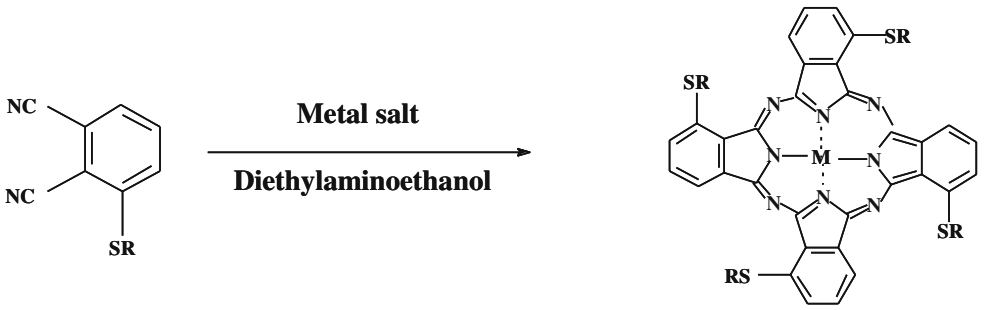


**1**

(AcO)Mn (**2**), Fe (**3**), Co (**4**) [28]

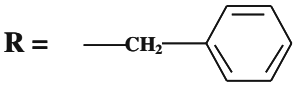


Hence, the type of substituent and the point of substitution on the Pc ring (peripheral or non-peripheral) will impact on the properties of the SAMs of MPc complexes. SAMs using CoPc or MnPc complexes peripherally substituted with benzylthio or dodecylthio groups have been reported [29, 30]. The complexes containing benzyl group formed less compact SAMs compared to the SAMs of the long chain derivatives. In this work, we report on the formation and characterization of SAMs of newly synthesized non-peripherally substituted benzylthio MPc complexes {*M*=Mn (**2**) or Fe (**3**)} and the previously reported CoPc derivative (**4**).

Electrocatalytic use of the SAM films was investigated for the electrocatalytic oxidation of the insecticide, carbofuran. Carbofuran is a systemic carbamate insecticide, employed in the control of insects in a wide range of field crops such as soybeans, potatoes, and corn [31]. It is significantly toxic, with toxicity comparable to that of parathion and aldicarb; hence, its electrocatalytic oxidation is relevant, as this will promote its detection in environmental samples. Carbofuran is not electroactive but the hydrolyzed derivative is electrochemically active (Scheme 2).

## Experimental

### Materials

Potassium carbonate, iron(II) chloride tetrahydrate, manganese(II) acetate, 2-diethylaminoethanol, and carbofuran were obtained from Sigma-Aldrich. Anhydrous form of iron(II) chloride was obtained by heating the hydrated form in an oven. Benzylmercapto thiol was obtained from Fluka. Tetrabutylammonium tetrafluoroborate ($TBABF_4$) (Aldrich) was used as the electrolyte for electrochemical experiments involving the complexes. Silica gel 60 (0.04–0.063 mm), for column chromatography, dimethylformamide (DMF), dichloromethane (DCM), and dimethyl sulphoxide (DMSO) were obtained from Merck. DMF, DMSO, DCM, methanol, and ethanol were distilled before use. Stock solution of carbofuran ($2.03\times10^{-3}$ mol$L^{-1}$) was prepared in freshly distilled methanol because of its low solubility in water. All solutions were prepared with ultrapure water of resistivity 18.2 MΩcm obtained from a Milli-Q Water system. Electrochemical experiments were carried out in argon-saturated aqueous solutions containing small amounts of methanol from the stock solution of carbofuran. Electrochemical analysis involving carbofuran was preceded by hydrolysis of a given volume of the stock solution in 0.5 mol$L^{-1}$ solution of NaOH. Acetic acid ($5\times10^{-5}$ L) was added to adjust the pH to 4; this pH gave the best voltammetry signal of carbofuran.

### Electrochemical studies

All electrochemical experiments were performed using Autolab potentiostat PGSTAT 302 (Eco Chemie, Utrecht, The Netherlands) driven by the general purpose Electrochemical System data processing software (GPES, software version 4.9) or BioAnalytical Systems (BAS) model 100B/

**Scheme 2** Hydrolysis of carbofuran in 0.5 mol$L^{-1}$ NaOH

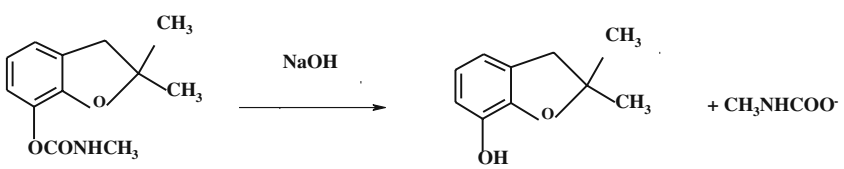

W Electrochemical Workstation (for rotating disc electrode, RDE voltammetry). Square wave voltammetric analysis was carried out at a frequency of 10 Hz; amplitude, 50 mV; and step potential, 5 mV. RDE studies were done in the potential range of 0.1–0.6 V at 200–500 rpm. A conventional three-electrode system was used. The working electrode was a bare glassy carbon electrode (for electrochemical characterization of the complexes) or polycrystalline gold disc electrode, having a geometric surface area of 0.02 $cm^2$ (for formation of SAMs), Ag|AgCl wire and platinum wire were used as the pseudo reference and auxiliary electrodes, respectively. The potential response of the Ag|AgCl pseudo-reference electrode was less than the Ag|AgCl (3 $molL^{-1}$ KCl) by 0.015± 0.003 V. Prior to use, the glassy carbon electrode surface was polished with alumina on a Buehler felt pad and rinsed with excess millipore water. The gold electrode surface was also polished in aqueous slurry of alumina on sic-emery paper and subjected to ultrasonic vibration in absolute ethanol to remove residual alumina. The electrode was then etched in hot 'piranha' solution (1:3 *v/v* 30% $H_2O_2$ and concentrated $H_2SO_4$) for 2 min, rinsed with excess millipore water and ethanol. It was then scanned in 0.5 $molL^{-1}$ $H_2SO_4$ between −0.5 and 1.5 V vs. Ag|AgCl to obtain a reproducible scan. The electrode was rinsed with freshly distilled DMF and placed in DMF containing the desired MPc complex ($1\times10^{-4}$ $molL^{-1}$) for a period of 24 h.

Spectroelectrochemical data were obtained using a home-made optically transparent thin-layer electrochemical (OTTLE) cell connected to a BAS CV 27 voltammograph.

### Equipment

UV/Vis spectra were recorded on Cary 50 UV/Vis/NIR spectrophotometer. Infrared (IR, KBr discs) spectra were recorded on Bruker Vertex 70-Ram II spectrophotometer. Elemental analysis was performed using Vario Elementar Microcube EL111. $^1H$ nuclear magnetic resonance (NMR, 400 MHz) was obtained in $CDCl_3$ using Bruker EMX 400 NMR spectrometer.

### Synthesis

#### *Manganese(III) acetate tetrakis-(benzylmercapto) phthalocyanine (non-peripheral) (**2**)*

3-(Benzylmercapto) phthalonitrile (compound **1**; Scheme 1), was synthesized as reported recently [28]. Complex **2** was synthesized using the method reported for the cobalt derivative [28]. A mixture of compound **1** (0.6 g, 1.85 mmol) and manganese(II) acetate (0.085 g, 0.49 mmol) was refluxed in 2-(diethylaminoethanol) (3 ml) for 8 h under nitrogen. The deep red crude product was cooled to room temperature and precipitated in excess methanol. The precipitate was filtered and dried in air. Purification was performed using column chromatography with silica gel as column material and $CHCl_3/CH_3OH$ (10:1) as eluent. Yield, 1.08 g (52%; found: C, 63.64%; H, 4.02%; N, 9.46%; S, 11.58%; Calc. for $C_{60}H_{40}N_8S_4MnOAc$: C, 64.06%; H, 3.56%; N, 9.96%; S, 11.39%); UV-Vis (DMF): $\lambda_{max}$ (nm) (log $\varepsilon$): 765 (5.5), 681 (4.8), 507 (4.6), 464 (4.6), 356 (5.2); IR (KBr) $\nu_{max}/cm^{-1}$; 3191–3067 (*w*, Ar-C-H), 1763, 1716, 1374, 1308, 1236, 1109, 1064

#### *Iron tetrakis-(benzylmercapto) phthalocyanine (non-peripheral) (**3**)*

Complex **3** was synthesized using the same method described above for complex **2** by replacing manganese(II) acetate with iron(II) chloride (0.062 g, 0.49 mmol). A deep green crude product was precipitated in excess methanol after cooling. The precipitate was filtered and dried in air. Purification was performed using column chromatography with silica gel as column material and $CCl_3/CH_3OH$ (10:1) as eluent. Yield, 0.92 g, (47%; found: C, 67.89%; H, 4.04%; N, 10.62%; S, 12.19%; Calc. for $C_{60}H_{40}N_8S_4Fe$: C, 68.19%; H, 3.79%; N, 10.61%; S, 12.12%); UV-Vis (DMF): $\lambda_{max}$ (nm) (log $\varepsilon$): 672 (5.4), 609 (5.0), 442 (5.2), 353 (5.6); IR (KBr) $\nu_{max}/cm^{-1}$; 3059–3025 (*w*, Ar-C-H), 2921 (*w*, $CH_2$) 1722, 1569, 1457, 1312, 1236, 1106, 743, 705.

## Results and discussion

### Synthesis

The pathway for the synthesis of complexes **2** and **3** is shown in Scheme 1. Cyclotetramerization of compound **1** took place in the presence of the desired salt (manganese(II) acetate for complex **2** and iron(II) chloride for complex **3**) to form the corresponding complex. Purification was accomplished using column chromatography on silica gel. The complexes were soluble in solvents such as DMF, DCM, and DMSO.

Characterization of the complexes was carried out using IR and UV-Vis spectroscopies as well as elemental analysis. The results obtained were consistent with the predicted structures shown in Scheme 1. Formation of the complexes was confirmed by the disappearance of the sharp $C\equiv N$ stretch at 2,229 $cm^{-1}$ [28] of **1**.

### UV-Vis spectral characterization of complexes **2** and **3**

Figure 1 shows the UV-Vis spectra of complexes **2** ($5.06\times10^{-6}$ $molL^{-1}$) and **3** ($4.25\times10^{-6}$ $molL^{-1}$) in DMF. Q band (765 nm) due to complex **2** was red-shifted compared to that due to complex **3** (672 nm). Generally, Q bands of MnPc complexes are red-shifted relative to that of other

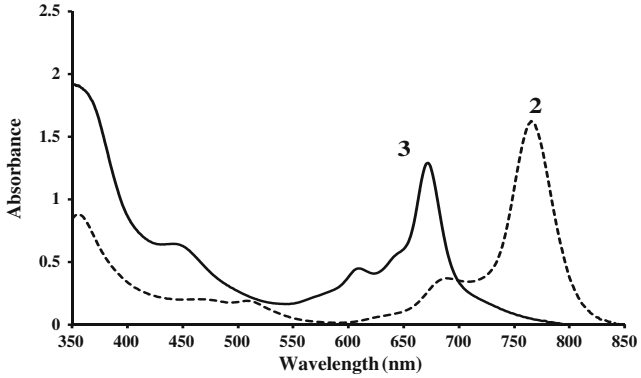


**Fig. 1** UV-Vis spectra of complexes **2** ($5.06\times10^{-6}$ mol$L^{-1}$) and **3** ($4.25\times10^{-6}$ mol$L^{-1}$) in DMF

metallophthalocyanine complexes [32]. For complex **2**, the B band envelope was observed at 356 nm while peaks at 464 and 507 nm are attributed to charge transfer bands. For complex **3**, peaks at 442 and 353 nm are characteristic of charge transfer and B band, respectively, while peak at around 638 nm can be associated with aggregation.

## Electrochemical and spectroelectrochemical characterizations of complex **2**

The square wave and cyclic voltammetry profiles of ~$1\times10^{-3}$ mol$L^{-1}$ of complex **2**, in freshly distilled DMF containing $TBABF_4$ supporting electrolyte, are shown in Fig. 2a and b. Two well-resolved redox processes (**I** and **II**) and one weak irreversible oxidation (**III***) process can be identified. Process **I** ($E_{1/2}$=−0.75 V versus Ag|AgCl) may be assigned to ring reduction and formation of $Mn^{II}Pc^{-2}$/$Mn^{II}Pc^{-3}$ species [33] while process **II** ($E_{1/2}$=−0.04 V versus Ag|AgCl) was attributed to metal-based reduction, $Mn^{III}Pc^{-2}/Mn^{II}Pc^{-2}$ [34] in comparison with literature, Table 1. Processes **I** ($\Delta E$=171 mV versus Ag|AgCl) and **II** ($\Delta E$=73 mV versus Ag|AgCl) were quasi-reversible and reversible, respectively. Ferrocene has $\Delta E$=70 mV versus Ag|AgCl at the same scan rate. Process **III*** ($E$p=+1.05 V versus Ag|AgCl) was a weak irreversible process assigned to ring oxidation ($Mn^{III}Pc^{-1}/Mn^{III}Pc^{-2}$), in comparison with literature [33]. Irreversible oxidation is a major feature of thio-substituted MPc complexes [35, 36]. At the concentrations employed for cyclic voltammetric studies, aggregation of MPc complexes is possible. Aggregation is evidenced in Fig. 2 by the broadening (partial splitting in square wave voltammograms) of the peaks. Aggregation in phthalocyanine complexes results in splitting of the voltammogram peaks [33]. These assignments were confirmed using controlled potential electrolysis performed in OTTLE cell.

Figure 3a shows the spectral changes observed on the application of potential slightly more negative of process **II**. The initial spectrum is slightly different (Q band: 768 nm) from the spectrum in Fig. 1 (Q band: 765 nm). The presence of electrolyte in the solution used for controlled electrolysis may be responsible for this difference. There was a blue shift in the Q band 768 to 710 nm (Fig. 3a) and collapse of the charge transfer band (509 nm) upon reduction. These spectral changes are consistent with metal-based reduction ($Mn^{III}$ to $Mn^{II}$) in MnPc complexes [32], supporting the assignment of process **II** to $Mn^{III}Pc^{-2}/Mn^{II}Pc^{-2}$ species. Although, manganese(II) acetate was used during synthesis, positions of the Q band in Figs. 1 and 3a suggest the formation of $Mn^{III}Pc$ species. The negative potential of the $Mn^{III}/Mn^{II}$ species makes it air sensitive, facilitating the oxidation of $Mn^{II}$ to $Mn^{III}$ during synthesis and purification [37]. The number of electrons transferred was estimated to be approximately 1 using Eq. 1

$$Q = nFVC \tag{1}$$

where, $n$, $F$, $V$, and $C$ are the number of electrons transferred, Faraday's constant, volume, and concentration of complex **2**, respectively.

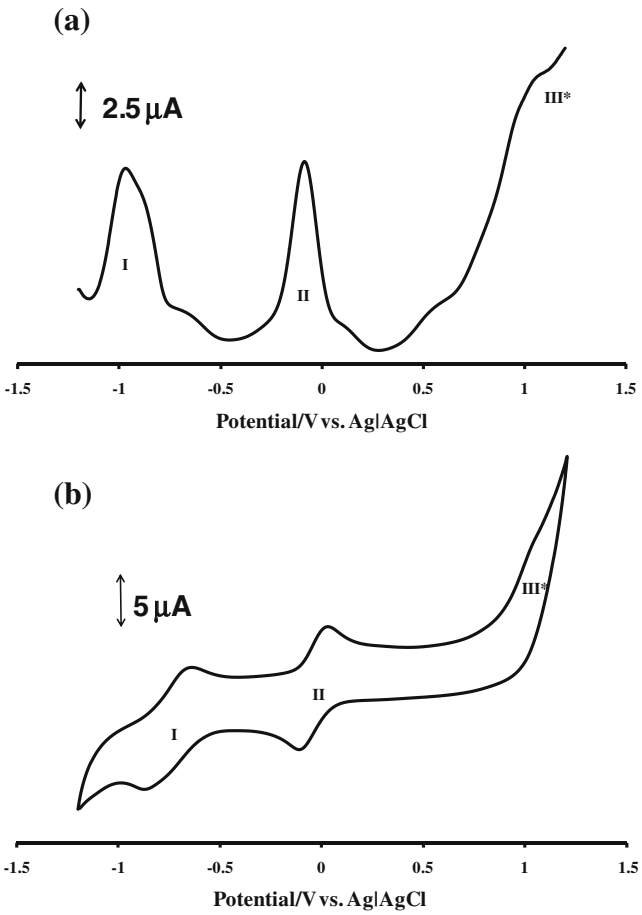


**Fig. 2** **a** Square wave and **b** cyclic voltammetry profiles of $1\times10^{-3}$ mol$L^{-1}$ of complex **2** in DMF; frequency, 10 Hz; amplitude, 50 mV; step potential, 5 mV; scan rate, 100 mV$s^{-1}$. Potentials versus Ag|AgCl pseudo reference

**Table 1** Electrochemical data of MnPc and FePc complexes

| MnPc complexes | | | | | |
|---|---|---|---|---|---|
| Complex[a] | $Mn^{II}Pc^{-2}/Mn^{II}Pc^{-3}$ | $Mn^{III}Pc^{-2}/Mn^{II}Pc^{-2}$ | $Mn^{III}Pc^{-1}/Mn^{III}Pc^{-2}$ | | Reference |
| **2** | −0.75 | −0.04 | +1.05 | | This work |
| (OH)Mn-$\beta$-TMPyPc | −0.71 | −0.057 | +1.34 | | 34 |
| (OH)Mn-$\alpha$-TMPyPc | −0.76 | −0.051 | +1.18 | | 34 |
| (OAc)Mn-$\beta$-TBMPc [b] | −0.98 | −0.26 | +0.83 | | 29 |
| FePc complexes | | | | | |
| Complex | $Fe^{I}Pc^{-2}/Fe^{I}Pc^{-3}$ | $Fe^{II}Pc^{-2}/Fe^{I}Pc^{-2}$ | $Fe^{III}Pc^{-2}/Fe^{II}Pc^{-2}$ | $Fe^{III}Pc^{-1}/Fe^{III}Pc^{-2}$ | |
| **3** | −1.11 | −0.64 | +0.22 | | This work |
| Fe-$\beta$-OPTPc | −0.70 | −0.26 | +0.25 | +0.60 | 43 |
| Fe-$\beta$-ODEAEPc[c] | −0.96 | −0.35 | +0.26 | +0.87 | 44 |

Half-wave ($E_{1/2}$) and peak ($E_p$) potentials in V vs. Ag|AgCl in DMF containing 0.1 $molL^{-1}$ $TBABF_4$

[a] *(OH)MnTMPyPc* (hydoxy) manganese tetra-(2-mercaptopyridine) phthalocyanine, *(OAc)Mn-α-TBMPc* (acetate) manganese tetra- benzylmercapto phthalocyanine, *FeODEAEPc* iron octakis-(2-diethylaminoethanethiol)-phthalocyanine, *FeOPTPc* iron octa phenylthio-substituted phthalocyanine

[b] Values recorded in DCM containing 0.1 $molL^{-1}$ $TBABF_4$

[c] Values recorded in DMF containing tetrabutylammonium perchlorate

The spectral changes in Fig. 3b were obtained on the application of potential slightly more negative of process **I**. There was further reduction of the species generated in Fig. 3a, resulting in decrease in intensity of the Q band and emergence of a new band around 530 nm. This indicates reduction of $Pc^{-2}$ to $Pc^{-3}$ [38], justifying the assignment of process **I** to the formation of $Mn^{II}Pc^{-2}/Mn^{II}Pc^{-3}$ species. The number of electrons transferred was evaluated to be 1 using Eq. 1. Confirmation of assignment of process **III*** was complicated by degradation of the complex (figure not shown) on the application of potential slightly more positive of this process. This is consistent with the behavior of thio-substituted MPc complex [39]. Nonetheless, assignment of process **III*** agrees closely with that reported previously for other MnPc complexes [29, 40] (Table 1).

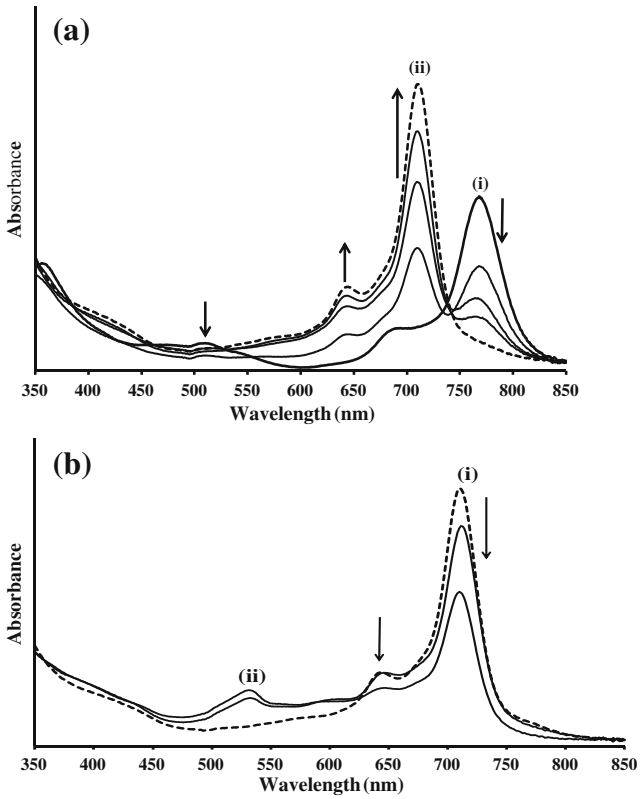


**Fig. 3** UV-Vis spectral changes observed for complex **2** during controlled potential electrolysis at **a** −0.1 V (process **II**), **b** −0.85 V (process **I**) vs. Ag|AgCl pseudo reference *i* spectrum before and *ii* spectrum after electrolysis. Electrolyte=DMF containing 0.1 $molL^{-1}$ $TBABF_4$. The final spectrum in **a** is the starting spectrum in **b**

## Electrochemical and spectroelectrochemical characterizations of complex 3

Figure 4a and b are the square wave and cyclic voltammetry profiles of $1\times10^{-3}$ $molL^{-1}$ of complex **3** in freshly distilled DMF containing $TBABF_4$ as supporting electrolyte. Three redox processes can be observed. Process **I** ($E_{1/2}$=−1.11 V versus Ag|AgCl) was reversible ($\Delta E$= 70 mV) in terms of cathodic to anodic peak separation, but the peak current ratio deviated from unity. This process is assigned to ring reduction and the formation of $Fe^{I}Pc^{-2}/Fe^{I}Pc^{-3}$ species [41]. Process **II** ($E_{1/2}$=−0.64 V versus Ag|AgCl) was also reversible ($\Delta E$=50 mV versus Ag|AgCl), it was attributed to metal-based reduction ($Fe^{II}Pc^{-2}/Fe^{I}Pc^{-2}$) [33]. Process **III** ($E_{1/2}$=+0.22 V versus Ag|AgCl) was a quasi-reversible ($\Delta E$=131 mV versus Ag|AgCl) metal-based oxidation assigned to $Fe^{III}Pc^{-2}/Fe^{II}Pc^{-2}$ species. No ring-based oxidation was observed in complex **3**. The voltammograms are affected by aggregation as was discussed above for complex **2**.

Figure 5 shows the spectral changes observed on the application of potential slightly more negative of process **II**.

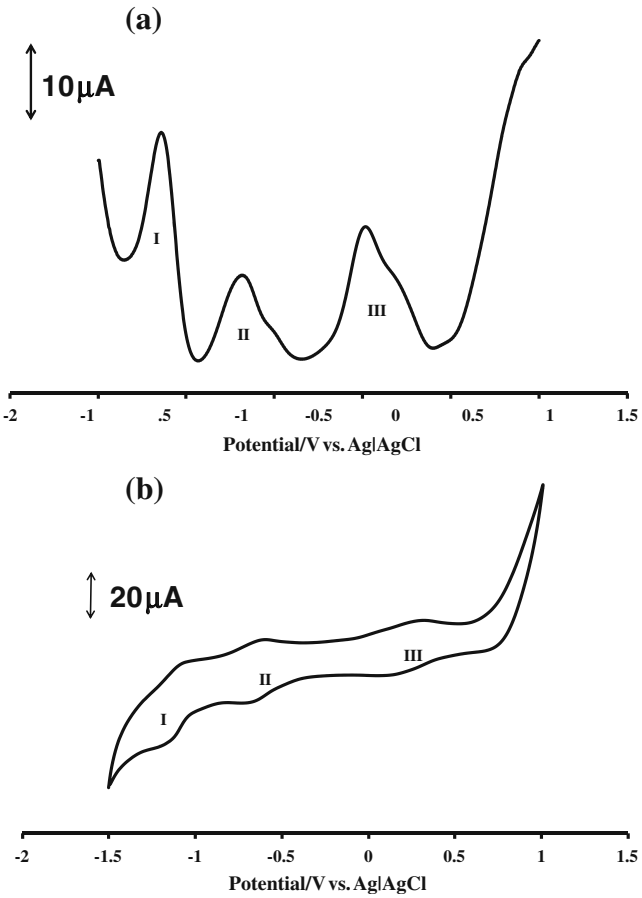


**Fig. 4** **a** Square wave and **b** cyclic voltammetry profiles of $1\times10^{-3}$ mol$L^{-1}$ of complex **3** in DMF; frequency, 10 Hz; amplitude, 50 mV; step potential, 5 mV; scan rate, 100 mV$s^{-1}$. Potentials versus Ag|AgCl pseudo reference

The first part involved shift in position of the Q band (670–676 nm), accompanied by a new band at 550 nm, Fig. 5a. The second part (Fig. 5b) shows intensification of the 550-nm band and formation of a pink solution. Reduction of $Fe^{II}Pc$ to $Fe^{I}Pc$ is known to show no Q band and to give a pink solution due to absorption in the 500-nm region [32]. The pink color of the solution has been attributed to disturbance of the π-π* spectrum of the phthalocyanine by $Fe^{I}$ [32, 42]. Hence, spectral changes in Fig. 5a and b confirm the assignment of process **II** to $Fe^{II}Pc^{-2}/Fe^{I}Pc^{-2}$ species. Assignment of process **I** and **III** are consistent with the data for other FePc complexes [43, 44] (Table 1).

## Formation and surface characterization of SAM films

SAM formation may be aided by the strong and specific interaction between gold and sulfur atoms of each of the complexes, without cleavage of C-S bond, as suggested previously [11]. For each complex, SAM formation was allowed for a period of 24 h.

## Characterization using cyclic voltammetry

Comparative cyclic voltammetry responses of the bare and SAM-modified gold electrodes in (a) 0.1 mol$L^{-1}$ KOH and (b) $1\times10^{-3}$ mol$L^{-1}$ $CuSO_4$ containing 0.5 mol$L^{-1}$ $H_2SO_4$, were used to characterize the SAM films. Considerable passivation of these redox processes was noticed on the SAM-modified gold electrodes, confirming formation of the SAM films.

Figure 6a shows cyclic voltammetry response of bare and SAM-modified gold electrodes in 0.1 mol$L^{-1}$ KOH. On the SAM-modified gold electrodes, there was a significant decrease in intensity of the gold oxide stripping peak at 0.02 V vs. Ag|AgCl. The gold oxidation process (near 0.3 V) is complicated by MPc redox processes. The extent of blocking by each SAM was evaluated by estimating the value of ion barrier factor using Eq. 2

$$\Gamma_{\mathrm{ibf}} = 1 - \frac{Q_{\mathrm{SAM}}}{Q_{\mathrm{Bare}}} \tag{2}$$

where, $Q_{\mathrm{SAM}}$ and $Q_{\mathrm{Bare}}$ ($1.82\times10^{-5}$ C) are the total charges (background corrected) under the reduction peak

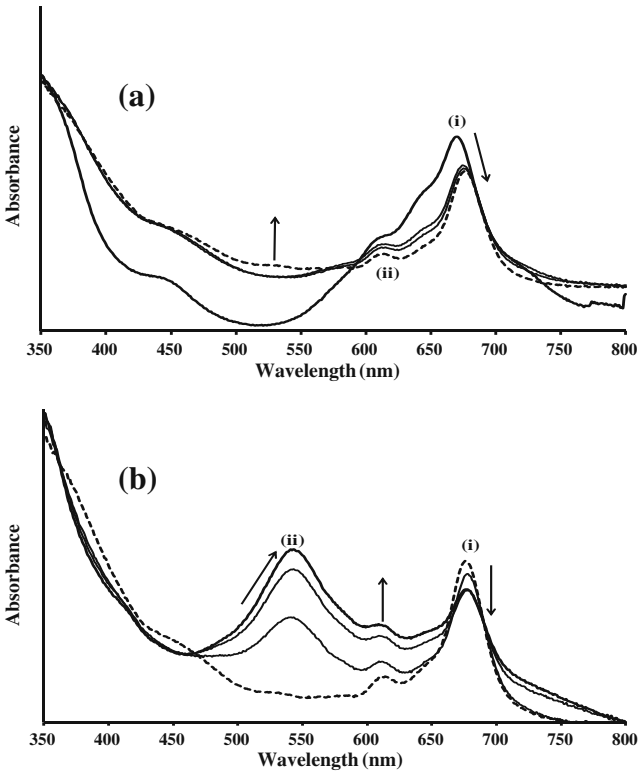


**Fig. 5** UV-Vis spectral changes observed for complex **3** during controlled potential electrolysis at ~−1.0 V (process **II**), vs. Ag|AgCl pseudo reference **a** initial changes and **b** final changes. *i* Spectrum before and *ii* spectrum after electrolysis. Electrolyte, DMF containing 0.1 mol$L^{-1}$ $TBABF_4$. The last spectrum in **a** in the same as the starting spectrum in **b**

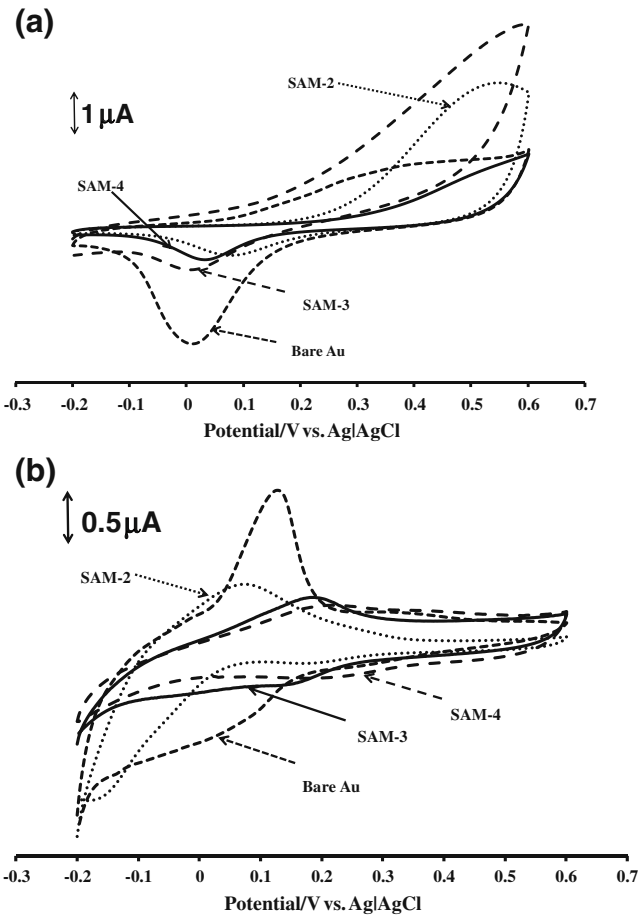


**Fig. 6** Cyclic voltammetry profiles of bare and MPc-SAM film-modified gold electrodes in **a** 0.1 $molL^{-1}$ KOH solution, **b** $1\times10^{-3}$ $molL^{-1}$ $CuSO_4$ solution containing 0.5 $molL^{-1}$ $H_2SO_4$. Scan rate, 25 $mVs^{-1}$. Potentials versus Ag|AgCl pseudo reference

(gold oxide stripping peak) on the SAM-modified and bare gold electrodes, respectively (Fig. 6a). In each case, the value obtained (0.76, 0.79, and 0.82 for SAM-**2**, SAM-**3**, and SAM-**4**, respectively; Table 2) suggests that SAM films have defects. In more closely packed SAM, with $\Gamma_{ibf}$ of ~1 [11, 30], the peak associated with gold oxide reduction is less pronounced, because the SAM is close to being defect-free. In principle, it is not possible to form a completely defect-free SAM, using the method employed in this study.

Cyclic voltammetry response of the bare electrode in 0.1 $molL^{-1}$ of KOH was also used for the estimation of the real or microscopic surface area of the electrode (discussed later).

Cyclic voltammetry profiles of bare (dashed) and SAM-modified gold electrodes in $1\times10^{-3}$ $molL^{-1}$ $CuSO_4$ containing 0.5 $molL^{-1}$ $H_2SO_4$ are shown in Fig. 6b. On bare gold electrode, both underpotential deposition and overpotential deposition of Cu are possible in the negative-going scan; hence, the stripping peak at +0.12 V (vs. Ag|AgCl) may be associated with both processes. These processes were substantially inhibited on the SAM-modified gold electrodes. The redox processes observed at $E_{1/2}$=+0.16 V, +0.20 V, and $E_p$=+0.06 V versus Ag|AgCl on SAM-**3**, **4**, and **2** modified gold electrodes, respectively, are metal-based redox processes of the respective films.

## Characterization of metal-based redox processes of the films

Metal-based redox processes of the adsorbed films were investigated for further characterization of the films. The observed processes (Table 2) were a reflection of the nature of the central metals of the MPc complexes constituting the films. Figure 7a show the cyclic voltammetry profile of SAM-**2**-modified gold electrode in pH 4 buffer solution. A well-resolved metal-based process ($E_{1/2}$=+0.02 V versus Ag|AgCl), attributed to $Mn^{III}/Mn^{II}$ species, was observed. This process was observed at $E_{1/2}$=−0.04 V versus Ag|AgCl in solution (Fig. 2b). Figure 7b and c are the cyclic voltammetry responses of SAM-**3** and **4**-modified gold electrodes, respectively, in pH 4 buffer solution. The redox process in Fig. 7b ($E_{1/2}$=+0.16 V versus Ag|AgCl) is attributed to $Fe^{III}/Fe^{II}$ species. In solution, this process was observed at $E_{1/2}$=+0.22 V versus Ag|AgCl (Fig. 4b). Apart from the differences in media (aqueous and DMF) and electrolytes (pH 4 buffer and $TBABF_4$), one of the major properties of chemically modified electrodes is that the formal potential of the surface-bound redox center is close to that of the solution derivative [4]. The $Co^{III}/Co^{II}$ redox process ($E$p=+0.17 V versus Ag|AgCl) observed in Fig. 7c was not as resolved as the redox processes in Fig. 7a and b. The difficulty in observing this process as adsorbed species is not surprising, it has been reported before that this process is difficult to observe as adsorbed species

**Table 2** Electrochemical parameters for SAM films of complexes **2**, **3**, and **4** in pH 4 buffer

| Electrode | $\Gamma_{ibf}$ | $M^{III}/M^{II}$ V vs. Ag\|AgCl | $\Gamma_{MPc\text{-}SAM}$/($molcm^{-2}$) | Reference |
|---|---|---|---|---|
| SAM-**2** | 0.76 | +0.02 | $6.9\times10^{-11}$ | This work |
| SAM-**3** | 0.79 | +0.16 | $4.8\times10^{-11}$ | This work |
| SAM-**4** | 0.82 | +0.17 | $1.8\times10^{-11}$ | This work |
| (OAc)Mn-$\beta$-TBMPc[a] | ~1 | + 0.27 | $0.66\times10^{-10}$ (18 h)[b] | 30 |
| Co-$\beta$-TBMPc[a] | ~1 | +0.32 | $1.1\times10^{-10}$ (24 h)[b] | 30 |

[a] *TBMPc* tetra- benzylmercapto phthalocyanine

[b] Numbers in brackets refer to time allowed for SAM formation

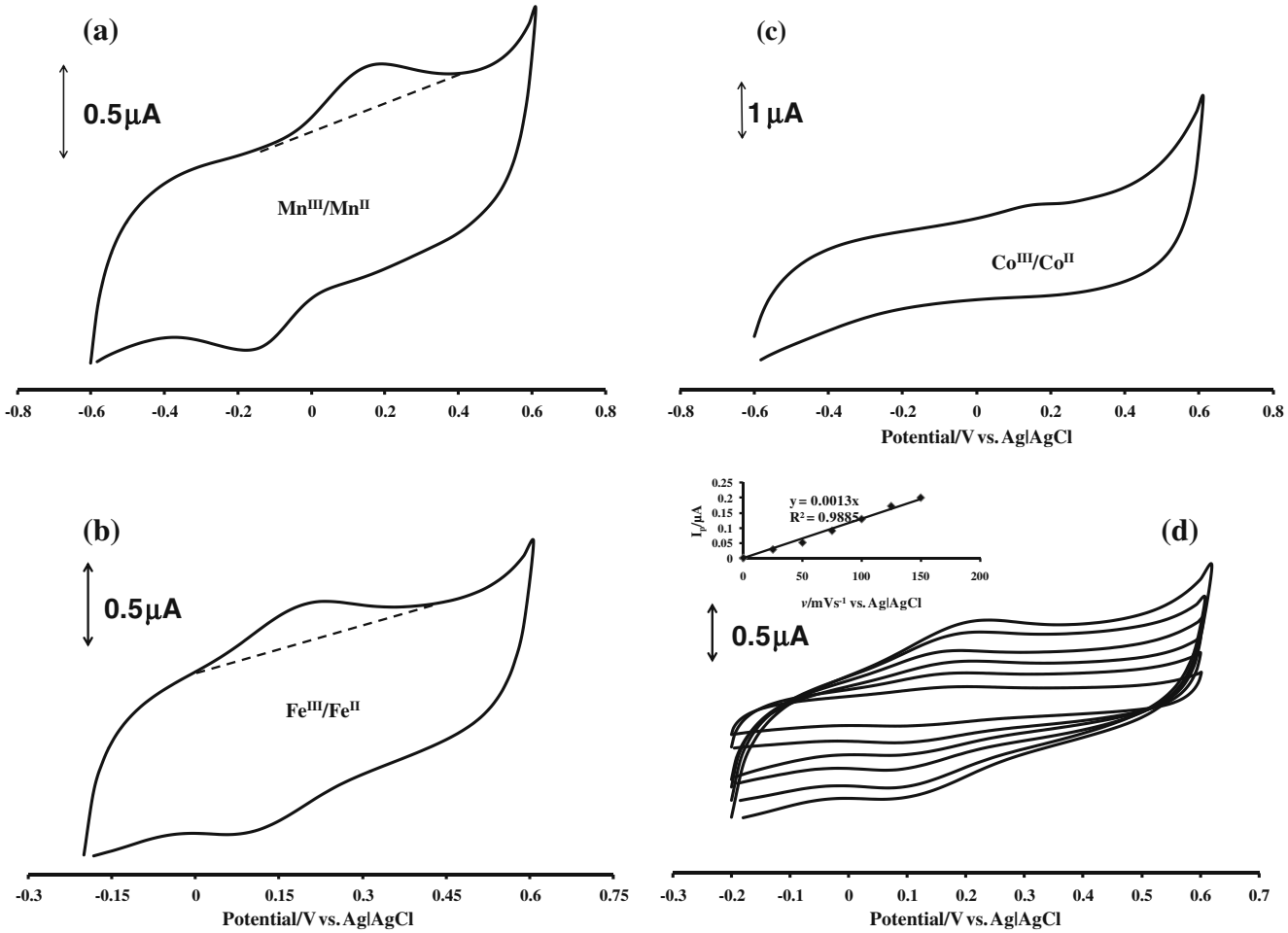


**Fig. 7** Cyclic voltammograms of **a** SAM-**2**, **b** SAM-**3**, and **c** SAM-**4**-modified gold electrodes in pH 4 buffer solution. Scan rate= 175 $mVs^{-1}$. Potentials versus Ag|AgCl pseudo reference. **d** Cyclic voltammograms of SAM-**3**-modified gold electrode at different scan rates (25–175 $mVs^{-1}$), inset is plot of peak current against scan rate

[45], making it unreliable in the estimation of surface coverage and likely orientation of the molecule of interest on a substrate.

For the corresponding peripherally substituted CoPc derivative (Co-β-TBMPc), the $Co^{III}/Co^{II}$ process was observed at +0.32 V versus Ag|AgCl in pH 4 buffer for the adsorbed complex, Table 2, suggesting this process is more energetically feasible on the SAM film of complex **4**. For the peripherally substituted MnPc derivative {(OAc)Mn-β-TBMPc}, $Mn^{IV}/Mn^{III}$ process was observed at +0.27 V, while in this work, there was no evidence of this process, $Mn^{III}/Mn^{II}$ process was observed at +0.02 V, instead of the $Mn^{IV}/Mn^{III}$ redox couple. Figure 7d shows the cyclic voltammetry profiles of SAM-**3**-modified gold electrode in pH 4 buffer at different scan rates (25–175 $mVs^{-1}$ versus Ag|AgCl). Linear dependence of peak current (anodic) on scan rate (inset in Fig. 7d), representative of other films, suggests surface confinement of the species constituting the films.

Surface concentration of each complex on the electrode was estimated using Eq. 3

$$\Gamma_{\mathrm{MPc-SAM}} = \frac{Q}{nFA} \tag{3}$$

where, $Q$ is the background corrected charge under the anodic peaks of the cyclic voltammetry responses in Fig. 7a–c ($3.1\times10^{-7}$, $2.1\times10^{-7}$, and $8\times10^{-8}$ C for SAM-**2**, **3**, and **4**, respectively), $n$ is the number of electrons transferred (=1), $F$ is Faraday's constant and $A$ is the real or microscopic surface area of the bare gold electrode.

The real surface area, $A$, of the electrode was determined using in situ method, involving measurement of oxygen adsorption. This method was reported in the review by Trasatti and Petrii [46]. As shown in Fig. 6a, oxygen is chemisorbed onto the bare gold electrode (forming an oxide layer) in the anodic potential scan, while the oxide layer is reduced in the cathodic scan [47]. The peak current, associated with the oxide formation,

suggests a monolayer of chemisorbed oxygen [47], such that a gold/oxygen ratio of 1:1 is assumed. Thus, the amount of surface oxide (estimate of the charge associated with its reduction) is a measure of the amount of gold atoms on the surface of the gold disc electrode. The value of charge required to reduce this oxide monolayer was calculated to be 400 $\mu C cm^{-2}$ on polycrystalline gold [46, 48]. This value is used widely in determining surface roughness. Using this value and the charge/geometric surface area (910 $\mu C cm^{-2}$) obtained in this work, the surface or microscopic roughness of the electrode was determined to be ~2.3, translating to a real surface area of 0.046 $cm^{-2}$ (roughness factor × geometric surface area).

Values of surface coverage obtained were $6.9\times10^{-11}$, $4.8\times10^{-11}$, and $1.8\times10^{-11}$ $mol cm^{-2}$ for SAM-**2**, **3**, and **4**, respectively (Table 2). Values of surface coverage calculated for all the SAM films are less than that expected for a monolayer ($1\times10^{-10}$ $mol cm^{-2}$) of a metallophthalocyanine or metalloporphyrin complexes lying flat on a substrate [49–51]. Low values of surface coverage have been reported for cobalt *meso*-tetrakis (4-pyridyl) porphyrin ($7.0\times10^{-11}$ mol $cm^{-2}$) [50] and cobalt tetrakis [*o*-(2-mercaptoethoxy)-phenyl] porphyrin ($4.76\times10^{-11}$ $mol cm^{-2}$) [52] adsorbed on gold electrode. SAM-**4** has lower value of surface coverage, compared to the corresponding peripherally substituted CoPc derivative (Co-β-TBMPc), Table 2, for the same number of hours used for SAM formation, attesting to the difficulty in forming SAMs using non-peripherally substituted derivatives. Hence, the low values of surface coverage obtained for the SAMs of the complexes studied in this work may be attributed to the non-peripheral position of the substituent. Also, the values of surface coverage do not reflect the extent of blocking (values of $\Gamma_{ibf}$, Table 2) characteristic of the SAMs. This may be attributed to the difference in the nature of packing of the molecules in the sub-monolayers.

## Electrocatalytic application of SAM films and mechanism of oxidation of carbofuran

Electrocatalytic application of the SAM films was investigated in the oxidation of the insecticide, carbofuran. Figure 8 shows the cyclic voltammetry responses of $2\times10^{-4}$ $mol L^{-1}$ solution of carbofuran, pH 4, on bare gold electrode (0.67 V, 0.74 μA) and the different films. Electrocatalysis was obvious from better carbofuran responses (less positive oxidation potentials and higher current responses; Table 3) on the SAM films 0.44 V, 1.81 μA on SAM-**2**; 0.37 V, 1.40 μA on SAM-**3**; and 0.51 V, 1.22 μA on SAM-**4** relative to that observed on bare gold electrode. Oxidation potentials of carbofuran on the SAM films suggest involvement of metal-based redox processes, Fig. 7a–c, in catalysis, since the catalytic peaks

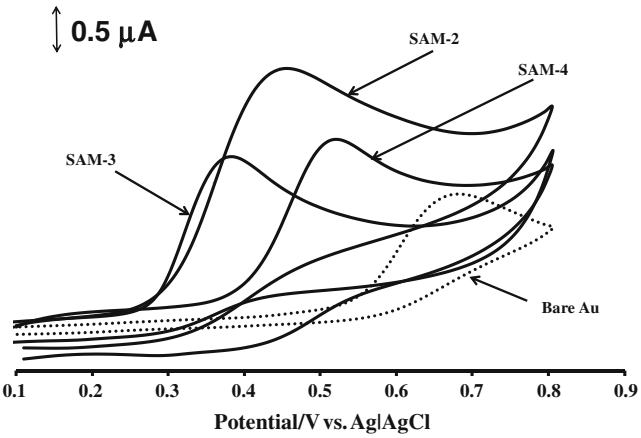


**Fig. 8** Cyclic voltammetry responses of bare (*dashed line*) and MPc-SAM Film modified gold electrode in $2\times10^{-4}$ $mol L^{-1}$ hydrolyzed solution of carbofuran (pH 4). Scan rate, 100 $mV s^{-1}$. The potential is versus Ag|AgCl pseudo reference electrode

are in the stability ranges of the $M^{III}/M^{II}$ couples. The absence of the anodic peak of the metal oxidation processes (near 0.2 for SAM-**3** or SAM-**4**) suggests that the metal oxidation products are consumed for the oxidation of carbofuran. Complex **3** is the best catalyst in terms of potential, since the lowest oxidation potential of carbofuran was observed on SAM film of this complex. It is important to mention that the electrode surface remained intact during the voltammetric measurements, since the surface could be re-generated by rinsing in acetone.

Mechanism of oxidation of carbofuran on the SAM films was elucidated using RDE voltammetry. Figure 9a shows the rotating disc electrode voltammograms obtained for the oxidation of $5\times10^{-4}$ $mol L^{-1}$ hydrolyzed solution of carbofuran on the SAM-modified gold electrodes at a rotation speed of 300 rpm. Tafel slopes, obtained from Tafel plots (plots of $\eta$ versus log $I_k$; Fig. 9b), were used to elucidate mechanism of oxidation of the insecticide. $I_k$ is the kinetic current corrected for mass transport ($I_k=(I\times I_L)/(I_L-I)$) and $\eta$ is overpotential (taken as the actual potential in this case). $I_L$ and $I$ are the limiting current (current obtained at 0.60 V for SAM-**2** and **3**, and at 0.48 V vs. Ag|AgCl for SAM-**4**) and the current at the foot of the wave respectively (Fig. 9a). $I_k$ is linearly related to overpotential (taken as the

**Table 3** Data for electrocatalytic oxidation of carbofuran on the SAM films

| Electrode | *E*p/V vs. Ag\|AgCl | *I*p/μA | Tafel slope/mV $decade^{-1}$ |
|---|---|---|---|
| SAM-**2** | 0.44 | 1.81 | 64 |
| SAM-**3** | 0.37 | 1.40 | 99 |
| SAM-**4** | 0.51 | 1.22 | 108 |
| Bare Au | 0.67 | 0.74 | |

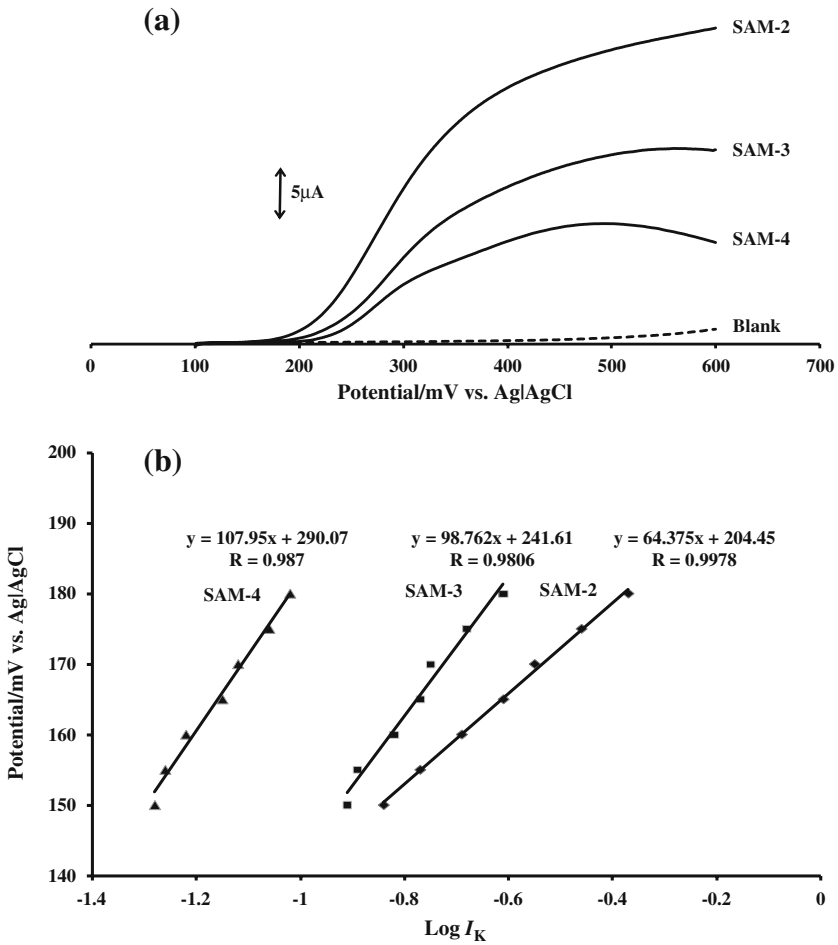


**Fig. 9** **a** RDE voltammograms and **b** Tafel plots for the oxidation of $5\times10^{-4}$ mol$L^{-1}$ solution of carbofuran, pH 4, at 300 rpm on the MPc-SAM film-modified gold electrodes, $I_k$ values were obtained from the RDE voltammograms in **a**

actual potential in this case) by the Tafel equation (Eq. 4).

$$\eta = a + b\log I_k \tag{4}$$

where $a$ is the Tafel constant, relating the exchange current density ($I_o$) and $b$ is the Tafel slope. Tafel slope ($b$) is defined by Eq. 5 [53]

$$b = 2.3\mathrm{RT}/\alpha n_a F \tag{5}$$

where, $n_a$ is the number of electrons involved in the rate-determining step and $\alpha$ is the electron transfer coefficient, also known as the symmetry factor. Exchange current density, $I_o$, is a measure of the rate of electrode reaction. A large $I_o$ is an indication of a fast reaction and vice versa.

Tafel slopes of approximately 64, 99, and 108 mV $decade^{-1}$ (Table 3) were obtained for the oxidation of carbofuran on SAM-**2**, **3**, and **4**, respectively. Tafel slopes within the range 60–120 mV $decade^{-1}$ suggests the rate-limiting step is a one-electron process and forecloses substrate–catalyst interaction. The mechanism below (Eqs. 6 and 7) is thus proposed for the oxidation of carbofuran on the SAM-modified gold electrodes. Oxidation potentials of carbofuran on the SAM films (Fig. 8) are within the stability range of the metal-based redox processes of the adsorbed films, thus the involvement of metal-based redox processes of the films (Fig. 7a–c) in catalysis. The proposed mechanism is as follows:

$$M^{II}Pc \rightarrow M^{III}Pc + e - (\mathrm{RDS}) \tag{6}$$

$$M^{III}Pc + RO^- \rightarrow M^{II}Pc + RO^{\cdot} \tag{7}$$

$R$ represents the remaining portion of the analyte (Scheme 2).

RDE voltammetry was also used to determine the heterogeneous rate constant-, $k$, for the oxidation of carbofuran on SAM-**2**-modified gold electrode (the SAM with best current signal of carbofuran; Fig. 8). Figure 10a show the RDE voltammograms obtained for the oxidation of carbofuran on SAM-**2**-modified gold electrode (representative of the other SAMs) at different rotation speeds (200–500 rpm). Inset is the plot of mass transport limiting current ($I_L$; obtained at 0.6 V versus Ag|AgCl) versus square root of rotation speed ($\omega^{1/2}$) in $rads^{-1}$. $I_L$ is linearly related to $\omega^{1/2}$,

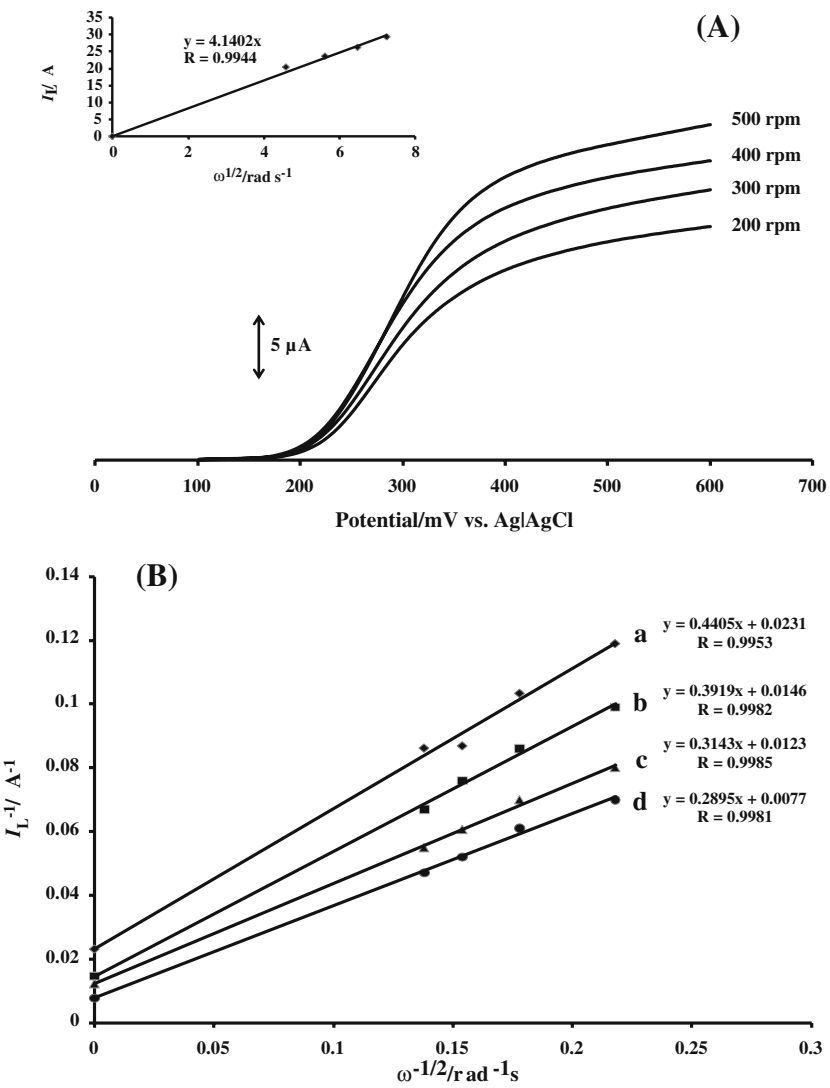


**Fig. 10** **A** RDE voltammograms for the oxidation of $5.0\times10^{-4}$ mol$L^{-1}$ carbofuran on SAM-**2**-modified gold electrode at different rotation speed (*inset*: Levich plot), and **B** Koutecky–Levich plots for the oxidation of carbofuran at different potentials: *a* 285, *b* 300, *c* 325, and *d* 350 mV vs. Ag|AgCl pseudo reference

with zero intercept, suggesting diffusion-controlled mass transport, predicated by the Levich equation (Eq. 8) [53]

$$I_L = 0.62nFAD^{2/3}\omega^{1/2}\upsilon^{-1/6}C \quad (8)$$

where $n$ is the number of electrons transferred during the oxidation of carbofuran (which is 1), $A$ (0.046 $cm^2$) is as defined previously, $C$ is the concentration of carbofuran ($5.0\times10^{-4}$ mol$L^{-1}$), $\upsilon$ is kinematic viscosity, and $D$ is diffusion coefficient of carbofuran in $cm^2s^{-1}$. The measured current ($I$) is defined by the Koutecky–Levich equation [53] (Eq. 9), which takes into account the mixed diffusion–kinetic regimes at intermediate potentials (first term) and mass transport limiting currents at high overpotentials (second term).

$$1/I = 1/(nFAkC) + 1/\left(0.62nFA\upsilon^{-1/6}D^{2/3}\omega^{1/2}C\right) \quad (9)$$

where $n$, $F$, $A$, and $C$ are as defined previously, while $k$ is the heterogeneous reaction rate constant. The first term in Eq. 9 represents the kinetic current ($I_k$), current in the absence of mass transport effect (Eq. 10)

$$I_k = nFAkC \quad (10)$$

Equation 9 predicts a linear dependence of $1/I$ on $\omega^{-1/2}$, with $1/I_k$ as intercept. Figure 10b are the plots of $1/I$ versus

**Table 4** Variation of kinetic current and heterogeneous rate constant with potential for the oxidation of 500 µM carbofuran on SAM-**2**-modified gold electrode

| *E*p/mV (vs. Ag\|AgCl) | $I_K$/A | $k$/cm$s^{-1}$ |
|---|---|---|
| 285 | $4.33\times10^{-5}$ | $1.95\times10^{-2}$ |
| 300 | $6.85\times10^{-5}$ | $3.08\times10^{-2}$ |
| 325 | $8.13\times10^{-5}$ | $3.65\times10^{-2}$ |
| 350 | $1.30\times10^{-4}$ | $5.85\times10^{-2}$ |

$\omega^{-1/2}$ for the oxidation of carbofuran on SAM-**2**-modified gold electrode, at different rotation rates (200–500), for each potential (285, 300, 325, and 350 mV) (a–d). Value of $I_k$ (Table 4) for each potential was evaluated from the intercept ($1/I_k$) of the corresponding plot of $1/I$ versus $\omega^{-1/2}$, and $k$ calculated using Eq. 10. An increase in the value of $k$ with increase in potential was observed (Table 4). An average value of $3.6\times10^{-2}$ cm s$^{-1}$ was obtained for $k$ on the SAM-**2**-modified gold electrode.

## Conclusions

Formation and surface characterization of self-assembled monolayer films of manganese (SAM-**2**), iron (SAM-**3**), and cobalt (SAM-**4**) phthalocyanine, non-peripherally tetra-substituted with benzylthio, are reported. Electrocatalytic property of the SAM films towards the oxidation of the insecticide, carbofuran has been investigated. Substantial passivation of redox processes, commonly associated with bare gold surface, confirmed formation of the SAM films. The films exhibited good electrocatalytic behavior towards the oxidation of the insecticide, carbofuran. Voltammetry responses of carbofuran were better on the SAM films than on bare gold electrode. In terms of less positive oxidation potential, the best catalytic activity towards carbofuran was observed on SAM film of the FePc derivative (**3**), while the best current signal of the insecticide was noticed on SAM-**2** film.

**Acknowledgments** This work was supported by the Department of Science and Technology (DST) and National Research Foundation (NRF) of South Africa through DST/NRF South African Research Chairs Initiative for Professor of Medicinal Chemistry and Nanotechnology and Rhodes University.

## References

1. Kitagawa K, Morita T, Kimura S (2005) Langmuir 21:10624–10631
2. Chen J, Reed MA, Rawlett AM, Tour JM (1999) Science 286:1550–1552
3. Ulman A (1991) An introduction to ultrathin organic films: from Langmuir–Blodgett to self-assembly. Academic Press, San Diego, pp 305–307
4. Finklea HO (1996) In: Bard AJ, Rubinstein I (eds) Electroanalytical chemistry, vol 19. Marcel Dekker, New York, pp 109–335
5. Finklea HO (2000) In: Meyers RA (ed) Encyclopedia of analytical chemistry: applications, theory and instrumentations, vol 11. Wiley: Chichester, pp 10090–10115
6. Cook MJ (1996) J Mater Chem 6:677–689
7. Simpson TRE, Russell DA, Chambrier I, Cook MJ, Horn AB, Thorpe SC (1995) Sens Actuators B 29:353–357
8. Gooding JJ, Praig VG, Hall EAH (1998) Anal Chem 70:2396–2402
9. Tian Y, Mao L, Okajima T, Ohsaka T (2004) Anal Chem 76:4162–4168
10. Retna RC, Ohsaka T (2003) J Electroanl Chem 540:69–77
11. Ozoemena KI, Nyokong T, Westbroek P (2003) Electroanalysis 15:1762–1770
12. Ozoemena K, Nyokong T (2002) Electrochim Acta 47:4035–4043
13. Ozoemena KI, Nyokong T (2005) Talanta 67:162–168
14. Ozoemena KI, Nyokong T (2006) Electrochim Acta 51:2669–2677
15. Whitten DG (1979) Angew Chem Int Ed Engl 18:440–450
16. Murray RW (1984) In: Bard AJ (ed) Electroanalytical chemistry, vol 13. Marcel Dekker: New York
17. Haller IJ (1978) J Am Chem Soc 100:8050–8055
18. Allara DL, Nuzzo RG (1985) Langmuir 1:45–52
19. Troughton EB, Bain CD, Whitesides GM, Nuzzo RG, Allara DL, Porter MD (1988) Langmuir 4:365–385
20. Porter MD, Bright TB, Allara DL, Chidsey CED (1987) J Am Chem Soc 109:3559–3568
21. Nuzzo RG, Fusco FA, Allara DL (1987) J Am Chem Soc 109:2358–2368
22. Liedberg B, Ivarsson B, Hegg P-O, Lundström I (1986) J Colloid Interface Sci 11:386–397
23. Cook MJ (1999) Pure Appl Chem 71:2145–2151
24. Simpson TRE, Revell DJ, Cook MJ, Russell DA (1997) Langmuir 13:460–464
25. Revell DJ, Chambrier I, Cook MJ, Russell DA (2000) J Mater Chem 10:31–37
26. Li Z, Lieberman M, Hill W (2001) Langmuir 17:4887–4894
27. Li Z, Liberman M (eds) (1999) Fundamental and applied aspects of chemically modified surfaces. J.P. Blitz and C.B. Little, Royal Soc. Chem., Lettchworth, U.K., pp 24-35
28. Akinbulu IA, Nyokong T (2010) Polyhedron 29:1257–1270
29. Agboola BO, Ozoemena KI, Nyokong T (2007) Electrochim Acta 52:2520–2526
30. Agboola B, Westbroek P, Ozoemena KI, Nyokong T (2007) Electrochem Commun 9:310–316
31. US Environmental Protection agency, Office of Pesticide Programs. Case number 0101
32. Stillman MJ, Nyokong T, Leznoff CC, Lever ABP (eds) (1989) Phthalocyanines: properties and applications, vol 1 (Chapter 3). VCH, New York, pp 133–290
33. Lever ABP, Milaeva ER, Speier G, Leznoff CC (eds) (1993) Phthalocyanines: properties and applications, vol 3. VCH Publishers, New York, pp 1–70
34. Sehlotho N, Durmuş M, Ahsen V, Nyokong T (2008) Inorg Chem Comm 11:479–483
35. Ozkaya AR, Gurek AG, Gul A, Bekaroglu O (1997) Polyhedron 16:1877–1883
36. Agboola BO, Ozoemena KI, Nyokong T (2006) Electrochim Acta 51:6470–6478
37. Leznoff CC, Black LS, Heibert A, Causey PW, Christendat D, Lever ABP (2006) Inorg Chim Acta 359:2690–2699
38. Mack J, Stillman MJ (2003) In: Kadish KM, Smith KM, Guilard R (eds) Phthalocyanines: spectroscopic and electrochemical characterization. The Porphyrin Handbook, vol 16, Chpt. 103. Academic Press, New York, pp 43-113
39. Takahashi K, Kawashima M, Tomita Y, Itoh M (1995) Inorg Chim Acta 232:69–73
40. Lever ABP, Minor PC, Wilshire JP (1981) Inorg Chem 20:2550–2553
41. Lever ABP, Wilshire JP (1978) Inorg Chem 17:1145–1151
42. Ban K, Nishizawa K, Ohta K, Shirai H (2000) J Mater Chem 10:1083–1090
43. Matemadomboa F, Maree MD, Ozoemena KI, Westbroek P, Nyokong T (2005) J Porphyr Phthalocyan 9:484–490
44. Akinbulu IA, Nyokong T (2009) Polyhedron 28:2831–2838
45. Griveau S, Pavez J, Zagal JH, Bedioui F (2001) J Electroanal Chem 497:75–83

46. Trasatti S, Petrii OA (1991) Pure Appl Chem 63:711–734
47. Oesch U, Janata J (1983) Electrochim Acta 28:1237–1246
48. Hoogvliet JC, Dijksma M, Kamp B, van Bennekom WP (2000) Anal Cem 72:2016–2021
49. Zagal JH, Guilppi MA, Depretz C, Lelievre D (1999) J Porphyr Phthalocyan 3:355–363
50. Hutchison JE, Postlethwaite TA, Murray RW (1993) Langmuir 9:3277–3283
51. Kobayashi N, Janda P, Lever ABP (1992) Inorg Chem 31:5172–5177
52. Van Galen DA, Majda M (1988) Anal Chem 60:1549–1553
53. Bard AJ, Faulkner LR (2001) Electrochemical methods: fundermentals and applications, 2nd edn. Wiley, New York